energy&fuels

pubs.acs.org/EF Article

Discovery of Oxygenated Hydrocarbon Biodegradation Products at a Late-Stage Petroleum Release Site

Olivia K. Bojan, Maria Irianni-Renno, Andrea J. Hanson, Huan Chen, Robert B. Young, Susan K. De Long, Thomas Borch, Thomas C. Sale, Amy M. McKenna, and Jens Blotevogel*

Cite This: *Energy Fuels* 2021, 35, 16713–16723 Read Online

ACCESS | Metrics & More | Article Recommendations | Supporting Information

ABSTRACT: The late stage of petroleum hydrocarbon releases to the subsurface is an evolving but largely unexplored concept. Herein, transmissive aquifer zones with little remaining petroleum liquids become attenuation zones for dissolved organic species released from low-permeability (low-k) zones *via* back diffusion. To address the knowledge gaps surrounding these subsurface zones, we explored a 40-year-old depleted petroleum body at a former refinery through high-resolution chemical and biomolecular analyses of a cryogenically collected soil core. 16S rRNA gene transcript-based analyses of active microbial communities uncovered predominately aerobic bacteria in the transmissive zone in contrast to anaerobic fermenting bacteria and methanogenic archaea in the low-k zone. Unexpectedly, Fourier-transform ion cyclotron resonance mass spectrometry (FT-ICR MS) analyses revealed a substantially higher degree of oxygenation in the petroleum biodegradation metabolites from the anoxic low-k zone compared to species in the oxic transmissive zone. Likely, a small diffusive influx of molecular oxygen enables limited aerobic metabolism in the low-k zone, while more abundant O_2 in the transmissive zone promotes rapid aerobic biodegradation of petroleum hydrocarbons without the accumulation of highly oxygenated intermediates. While much remains to be uncovered, our work is a critical first step toward enabling better-informed decision making regarding best management practices for late-stage petroleum hydrocarbon-impacted sites.

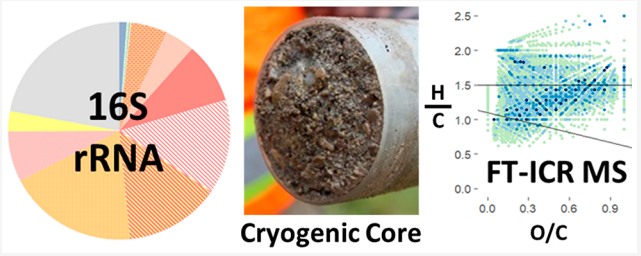

INTRODUCTION

Subsurface releases of petroleum liquids are among the most common causes of soil and groundwater contamination in the world. Spills can range in size from 10s to 100 000s of cubic meters at various sites from retail to refining facilities. Typically, a substantial share of subsurface light nonaqueous phase liquids (LNAPLs) are biodegraded anaerobically to CO_2 and CH_4 through natural source zone depletion (NSZD) processes.[1−5] Biogenic gases migrate upward through off-gassing and ebullition to the vadose zone where the methane is mineralized by methanotrophs using downward-diffusing atmospheric oxygen.[5−7] The fate of subsurface petroleum liquids follows the short-term carbon cycle wherein C−H bonds are iteratively replaced with C−O bonds and ultimately oxidized to CO_2, which cycles back into organic compounds *via* photosynthesis.

Subsurface petroleum releases evolve with time.[8] Early stage releases are largely about expanding pools of unaltered LNAPLs in transmissive zones of the aquifer. At early stage sites, active recovery efforts are commonly employed to deplete LNAPL to the extent practicable.[9] With time, NSZD and active recovery efforts transform early stage LNAPL sites into middle-stage sites, where continuous LNAPL is largely depleted, while dissolved-phase total petroleum hydrocarbons (TPH) as well as benzene, toluene, ethylbenzene, and xylenes (BTEX) persist in groundwater. Soluble species move into low-permeability (low-k) zones within the aquifer *via* slow advection and diffusion. Given the limited efficacy of active remedies at middle-stage sites, NSZD often emerges as the primary factor driving the maturation of LNAPL sites with reported rates of cleanup due to NSZD ranging from 1000s to 10 000s of liters per hectare per year.[10]

The late stage of petroleum releases is an evolving but largely unexplored concept wherein (1) much of the remaining contaminant mass remains in low-k zones, and (2) transmissive zones, with little to no remaining petroleum liquids, become attenuation zones for species released from low-k zones *via* back diffusion. Contaminants diffusing out of low-k zones can become a persistent secondary source long after the primary source has been removed.[11] Of emerging scientific, engineering, and regulatory concerns are oxygenated hydrocarbon

Received: August 2, 2021
Revised: September 22, 2021
Published: October 6, 2021

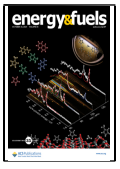

https://doi.org/10.1021/acs.energyfuels.1c02642
Energy Fuels 2021, 35, 16713−16723

transformation products, sometimes referred to as "polar hydrocarbons", "oxyhydrocarbons", or "petroleum biodegradation metabolites". Oxygen-containing metabolites such as organic acids, esters, alcohols, phenols, aldehydes, and ketones are generated through biologically mediated "weathering" processes.[12] Partially oxidized petroleum metabolites can comprise up to 100% of the extractable organic carbon in the downgradient groundwater plume[2,13,14] with a principal concern being increased water solubility and mobility of metabolites in aqueous environments.[15−17]

However, the significance and prevalence of oxygenated hydrocarbon metabolites in groundwater are insufficiently understood, constrained by limited data and analytical challenges. Most often, only TPH and BTEX are analytically quantified using gas chromatography (GC)-based methods. While TPH may be a useful bulk parameter for the characterization of the nonpolar LNAPL fraction, this GC-based analysis is not suitable for the detection of low-volatility, high-molecular weight transformation products.[18,19] Consequently, recent research has applied (ultra)high-resolution mass spectrometry, sometimes coupled with chromatographic separation, to investigate the fate of dissolved hydrocarbon weathering products in downgradient groundwater plumes.[16,20,21] The interdependence of oxygenated hydrocarbon metabolites and microbial ecophysiology is one of the keys to understanding the late-stage processes leading to site cleanup and ultimately forecasting the time to site closure. Yet, molecular insights into the nature and release of organic carbon from aged LNAPL source zones along with knowledge pertaining to the active microbial communities largely driving transformation processes are critically missing.

Herein, we uniquely explore a late-stage petroleum hydrocarbon-contaminated site in both transmissive and low-k zones at the upgradient edge of a 40-year-old depleted petroleum LNAPL body at a former refinery. Our work was motivated by the vision that an enhanced understanding of the nature of late-stage sites will support better-informed decisions regarding best management practices for middle- and late-stage petroleum LNAPL sites. First, we collected a cryogenic soil core for subsequent high-resolution stratigraphic and chemical characterization. In contrast to traditional soil coring methods, such as direct push or hollow-stem auger drilling, cryogenic coring with a liquid nitrogen cooling system improves core recovery and preserves critical soil attributes such as pore fluid distribution[22,23] and ribonucleic acid content.[24] Second, we sought to define the prevailing redox conditions in the low-k and transmissive zones governing hydrocarbon biodegradation through determining the active microbial community composition *via* 16S rRNA gene transcript analysis as opposed to traditional DNA-based microbial community profiling. Third, we applied Fourier-transform ion cyclotron resonance mass spectrometry (FT-ICR MS) to highlight compositional differences in acidic and aromatic species between soil samples originating from transmissive and low-k zones. FT-ICR MS achieves unrivaled resolving power and mass accuracy and thus provides unprecedented molecular-level details for the characterization of petroleum-derived compounds.[18] Results suggest that, much like chlorinated solvent sites, the late stages of petroleum LNAPL sites will be defined by processes in and about low-k zones.

EXPERIMENTAL SECTION

Field Site Characterization and Soil Core Sampling. Between 1931 and 1986, gasoline, jet fuel, diesel, and heating oil were produced from crude oil at the study site, a former refinery. Standard practices of the era of operations had caused inadvertent releases of substantial volumes of petroleum liquids to the subsurface, leading to a largely contiguous body of LNAPL about the water table beneath the ∼1 km^2 former refinery. The site is situated above a high transmissivity glacial valley train aquifer near the terminus of continental glaciation in the central U.S. High-transmissivity sands and gravel beds (high-flow summer glacial melt deposits) are interbedded with low-k silts (low-flow winter deposits). Inclusive to the aquifer is a large river that is in direct hydraulic connection with the aquifer. Groundwater fluctuations on the order of 3−7 m follow the river stage.

In August of 2016, 6 cm outer diameter (OD) cryogenic soil cores were collected from the upgradient edge of the depleted petroleum LNAPL body following the steps illustrated in Figure S1 (Supporting Information). Core was collected continuously in six 76 cm intervals (drives) about the water table, from 7.4 to 10.5 m below ground surface (bgs). Soil cores were frozen *in situ* using a dual-wall closed-loop cooling barrel inside a standard CME continuous sample tube system for 11 cm inner diameter (ID) hollow stem augers drill systems. Details of the cryogenic sampling tool and associated drilling methods are documented in ref 23. The core was shipped overnight on dry ice to Colorado State University, Fort Collins, Colorado, and stored at −80 °C until processing.

Sample Preparation. The frozen soil cores were cut into 2 cm thick cylinders ("hockey pucks") at 5 cm intervals. The hockey pucks were quartered into subsamples for analyses of petroleum hydrocarbons, soil gases, and microbial community from the same depth interval following methods described by Olson et al. in 2017.[25] For high-resolution hydrocarbon analysis, the frozen samples (including any frozen water) were thawed and extracted with HPLC-grade toluene in a wide-mouthed glass jar on a mechanical shaker for at least 2 h. Toluene was chosen as the extraction solvent to minimize interferences from nonpetroleum hydrocarbons.[26] Toluene extraction of spiked samples showed (near-) complete recovery of diesel range organics at 104 ± 6% and of decanoic acid, a surrogate for polar hydrocarbons, at 108 ± 7%. Subsamples for methane analysis were placed frozen in jars containing deaired deionized water as described in Olson et al.[25] Subsamples for TPH analysis were thawed and extracted with methanol.

Analytical Methods. Methanol extracts were transferred to 2 mL vials and analyzed for TPH including benzene on an Agilent 6890N gas chromatograph (Agilent Technologies, Santa Clara, CA) equipped with a flame ionization detector (GC/FID) and a Restek Rtx-5 column (30 m length × 0.32 mm inner diameter × 0.25 μm film thickness, Bellfonte, PA). Aqueous extracts were analyzed for methane *via* headspace analysis on an Agilent 6890N gas chromatograph (Agilent Technologies, Santa Clara, CA) equipped with an FID, following methods described by Olson et al. in 2017.[25]

Toluene extracts to be analyzed by FT-ICR MS were desolvated in preweighed borosilicate dried under nitrogen gas for analysis at the National High Magnetic Field Laboratory in Tallahassee, FL. All solvents were HPLC-grade (Sigma-Aldrich Chemical Co., St. Louis, MO).

Samples were dissolved in toluene to a final concentration of 125 μg/mL for positive-ion atmospheric pressure photoionization ((+)APPI) FT-ICR MS at a flow rate of 50 μL/min.[27] An APPI source (Thermo-Fisher Scientific, San Jose, CA) was coupled to the first stage of a custom-built FT-ICR mass spectrometer (see below) through a custom-built interface.[27] (+)APPI was chosen to target aromatic and less polar compounds. The tube lens was set to 50 V (to minimize ion fragmentation) and the heated metal capillary current was 4.5 A. A Hamilton gastight syringe (5.0 mL) and syringe pump were used to deliver the sample (50 μL/min) to the heated vaporizer region (350 °C) of the APPI source, where N_2 sheath gas (50 psi) facilitates nebulization. The auxiliary port remained plugged. After

https://doi.org/10.1021/acs.energyfuels.1c02642
Energy Fuels 2021, 35, 16713−16723

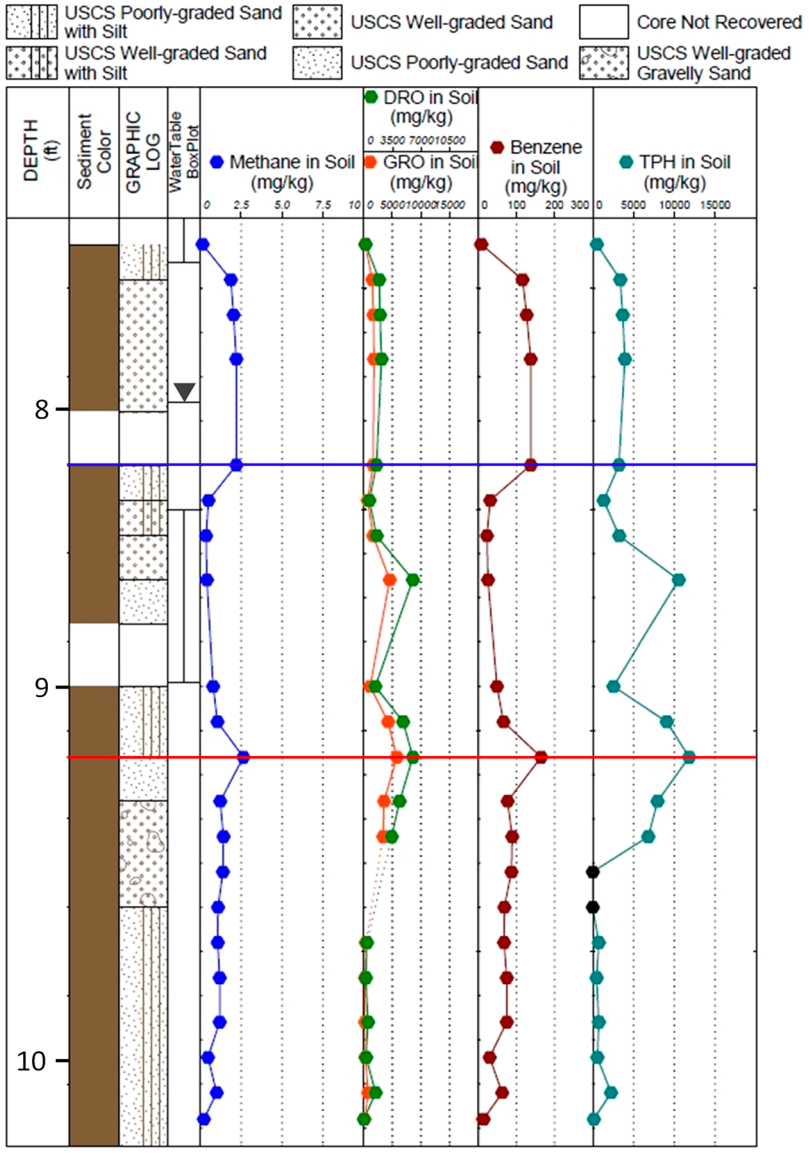

Figure 1. Graphic log of the cryogenically collected core illustrating sediment color, soil classification, water level, methane, and petroleum hydrocarbon component concentrations as a function of depth below ground surface. The blue and red lines indicate the locations at which the low-k zone and the transmissive zone samples were taken, respectively.

nebulization, gas-phase neutral analyte molecules exit the heated vaporizer region as a confined jet. A krypton vacuum ultraviolet gas discharge lamp (Syagen Technology, Inc., Tustin, CA) produces 10−10.2 eV photons (120 nm). Toluene increases the ionization efficiency for nonpolar aromatic compounds through dopant-assisted APPI through charge exchange and proton transfer reactions between ionized toluene molecules and neutral analyte molecules as previously reported.[28−32]

For electrospray ionization (ESI) analysis, samples were reconstituted in toluene and then dissolved in methanol to a final concentration of 150 μg/mL in Tol/MeOH (1/1). Once dissolved in solvent, oil samples were acidified with formic acid to a final concentration of 2% acid (v/v) and 0.0125% tetramethylammonium hydroxide (TMAH) by volume for negative electrospray ionization ((−)ESI) at a flow rate of 500 nL/min.[33] (−)ESI was selected to target carboxylic acids and other polar functional groups.

All samples were analyzed with a custom-built FT-ICR mass spectrometer[34] equipped with a 22 cm horizontal room temperature bore 9.4 T superconducting solenoid magnet (Oxford Instruments, Abingdon, U.K.), and a modular ICR data station (Predator)[35] facilitated instrument control, data acquisition, and data analysis. Positive ions generated at atmospheric pressure enter the skimmer region (~2 Torr) through a heated metal capillary, pass through the first radiofrequency (rf)-only octopole, pass through an rf-only quadrupole, and are externally accumulated[36] (25−50 ms) in a second octopole equipped with tilted wire extraction electrodes for improved ion extraction and transmission.[37] Helium gas introduced during accumulation collisionally cools ions prior to transfer through rf-only quadrupoles (total length 127 cm) (into a seven-segment open cylindrical cell with capactively coupled excitation electrodes on the basis of the Tolmachev configuration.[38,39] One hundred individual transients of 6.8 s duration were signal averaged. The data was collected at the maximum memory depth of the data station hardware (16 million samples), apodized with a single sided Hanning apodization, zero-filled to 16 megasample (16 777 216 samples or 224). An additional zero fill brings the preFT data packet to 32 megasample, which in turn is processed *via* absorption-mode FT analysis.[40,41] Experimentally measured masses were converted from the International Union of Pure and Applied Chemistry (IUPAC) mass scale to the Kendrick mass scale[42] for the rapid identification of homologous series for each heteroatom class (i.e., species with the same $C_cH_hN_nO_oS_s$ content, differing only by degree of alkylation).[43]

https://doi.org/10.1021/acs.energyfuels.1c02642
Energy Fuels 2021, 35, 16713−16723

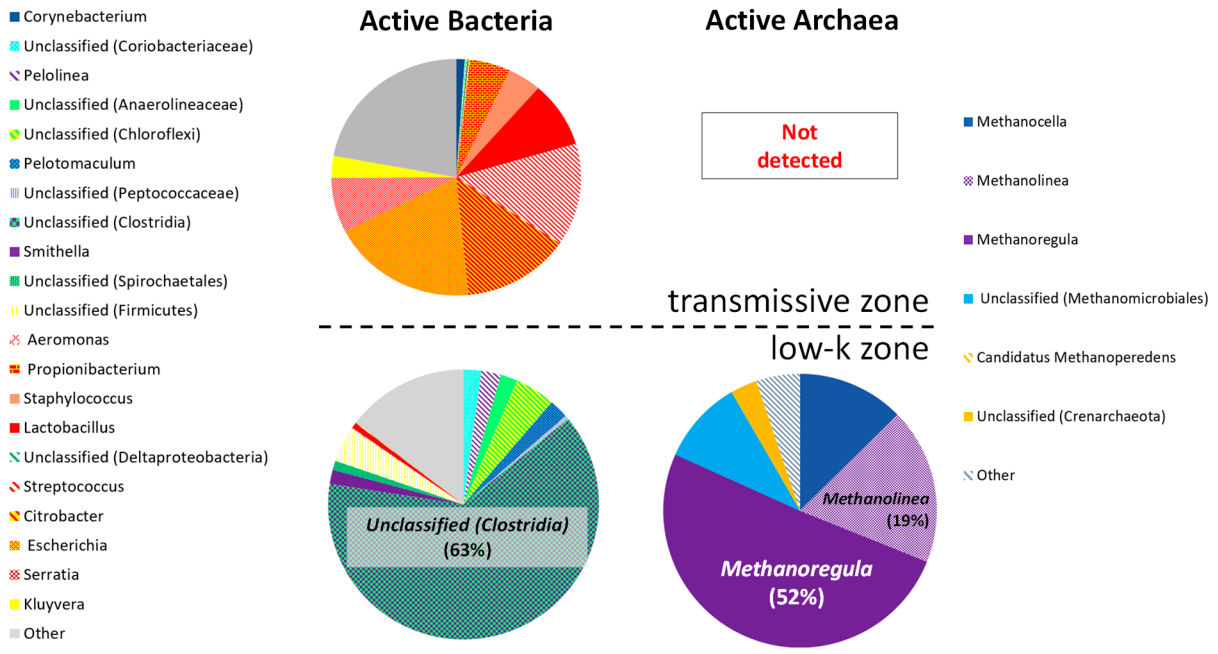

Figure 2. Active microbial community composition and relative abundances in the oxic transmissive zone and in the anoxic low-k zone. Assignments were made at the genus level; in cases where genera were unclassified, higher level taxonomic identifications are reported, but grouped taxa shared >95% sequence similarity. Not detected indicates that no amlicon could be generated for sequencing.

For each elemental composition, $C_cH_hN_nO_oS_s$, the heteroatom class, type, double bond equivalents (DBEs), and carbon number were tabulated for subsequent generation of heteroatom class relative abundance distributions and graphical relative-abundance weighted DBE versus carbon number images. Peaks with a signal magnitude greater than 6 times the baseline root-mean-square noise at m/z 500 were exported to peak lists, internally calibrated based on the "walking calibration",[44] and molecular formula assignments and data visualization were performed with PetroOrg software.[45] Molecular formula assignments with an error >0.5 ppm were discarded, and only chemical classes with a combined relative abundance of ≥0.15% of the total were considered. For all mass spectra, the achieved spectral resolving power approached the theoretical limit over the entire mass range: for example, the average resolving power, $m/\Delta m_{50\%}$ in which $\Delta m_{50\%}$ is the mass spectral peak full width at half-maximum peak height, was ∼1 000 000−1 500 000 at m/z 500.

All raw FT-ICR mass spectra files and complete elemental compositions are publically available *via* the Open Science Framework at https://osf.io/pt8gh/.

Characterization of Active Microbial Communities. To probe microorganisms that were active at the time of sampling, as opposed to overall microbial community composition, this study targeted ribonucleic acid (RNA), which is only produced by metabolically active cells. Samples from two intervals were selected for detailed differential characterization based on representing two distinct hydrogeologic zones and the presence of a substantial TPH concentration (Figure 1). RNA was extracted from each soil sample with a Powerlyser Powersoil DNA Isolation Kit (MoBio, Carlsbad, CA) generally according to the manufacturer's instructions but with a modified protocol that preserves intact RNA and removes molecules that interfere with downstream analysis of extracted RNA (i.e., polymerase chain reaction inhibitors) while maximizing yield.[6,24] RNA concentrations were quantified *via* optical density with a NanoDrop 2000 UV−vis spectrophotometer (Thermoscientific). RNA was stored at −80 °C prior to it being reverse transcribed into complementary DNA (cDNA) for downstream analysis.

To gain information regarding all types of bacteria and archaea active in the subsurface at the time of sampling, cDNA obtained from extracted RNA was used for 16S rRNA amplicon sequencing *via* next generation sequencing (Illumina MiSeq). Sequencing was performed by Research and Testing Laboratories, LLC (Lubbock, TX) using an Illumina MiSeq System (Illumina, San Diego, CA). 16S rRNA community profiling was performed with bacterial primers 28F and 519r and archaeal primers 517f and 909r.[46,47]

The Ribosomal Database Project (RDP) classifier was used in conjunction with the Silva database for taxonomic placement of the 16S rRNA gene sequences analyzed (https://www.arb-silva.de/). Relative abundance (%) data generated by high throughput sequencing was used to construct pie charts that present microbial community composition for each sample. Analyses were conducted at the genus level. In cases where genera could not be classified, higher level taxonomic identifications are reported, but grouped taxa shared >95% sequence similarity. Genera that individually represented less than 3% of the microbial communities were combined and reported as "other".

RESULTS AND DISCUSSION

Soil Core Characterization. Figure 1 presents a gINT plot illustrating the soil core log and concentration data collected from 21 subsamples between 7.4 and 10.5 m bgs. Core was recovered from 88% of the sample intervals, with recovery occasionally being inhibited by cobbles larger than the 6 cm outer diameter (OD) of the core barrel. Geologic logging revealed a transmissive medium- to coarse-grained sand at 9.3 m bgs and a low-k zone at 8.2 m bgs composed of gravel infilled with silt (panels 6, 7, and 8 in Figure S1). Samples from these two intervals were used to explore differences in active microbial ecologies and hydrocarbon speciation between transmissive and low-k zones. TPH concentrations in the low-k and transmissive zones were 3170 and 11 775 mg/kg, respectively, with observed residual LNAPL and diesel range organics (DRO) to gasoline range organics (GRO) ratios slightly greater than one in both samples.

At a mean water table depth of 8.0 m bgs, the low-k zone is located within the range of natural groundwater table fluctuations. However, there is no inflow of atmospheric oxygen to the low-k zone due to an overlying layer of methane from anoxic hydrocarbon biodegradation, where methano-

https://doi.org/10.1021/acs.energyfuels.1c02642
Energy Fuels 2021, 35, 16713−16723

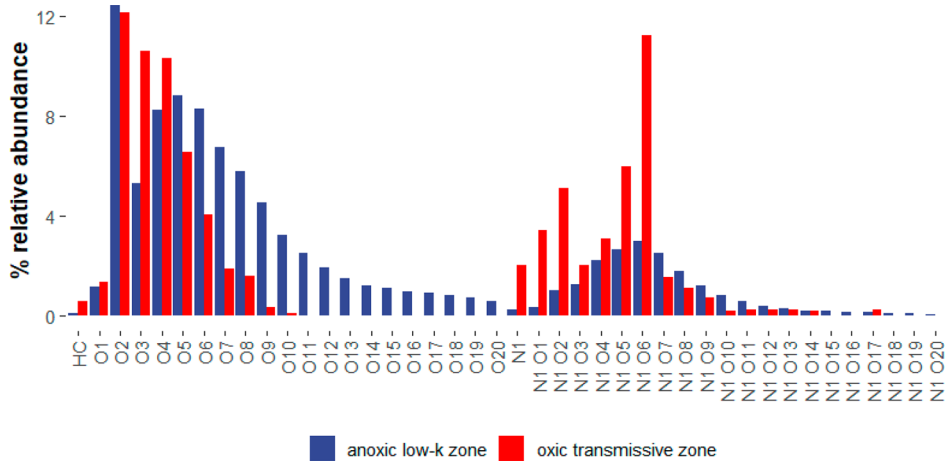

Figure 3. Heteroatom class distribution derived from (−)ESI FT-ICR MS for toluene-soluble extracts in the anoxic low-k (blue) and oxic transmissive (red) zones.

trophic microorganisms use any downward-diffusing oxygen as electron acceptor.[7] This was reflected by a concentration of 2.18 mg/kg of methane. In contrast, the transmissive zone experiences a constant influx of dissolved oxygen from the nearby river. Nevertheless, methane was detected here at 2.62 mg/kg methane, likely due to methane production at greater depths and subsequent vertical transport of the ebullient gases through layers of higher permeability.[4]

Active Microbial Community Analysis Reveals Predominant Redox Conditions. To acquire a better representation of the prevalent redox environment in both the transmissive and low-k zones, and to broadly relate metabolic processes to the hydrogeochemical conditions, we conducted 16S rRNA gene transcript sequencing from select samples. We note that this microbial community composition analysis was limited to RNA only, and sequencing was performed on only one representative sample from each respective zone; thus, we obtained only a snapshot of the overall microbial community in a highly heterogeneous system.

Nevertheless, as visible in Figure 2, distinctly different active microbial communities were established in the transmissive zone compared to the low-k zone. In the transmissive zone, aerobic microorganisms comprised over 75% of the assigned phylotypes for the active bacterial community. Coupled with nondetectable archaea in this zone, these findings corroborate the presence of oxygen here and establish the transmissive zone as oxic and conducive to aerobic hydrocarbon degradation. Moreover, several assigned phylotypes have been previously associated with aerobic hydrocarbon degradation. For instance, members of the genus *Kluyvera* have been associated with aerobic benzene and naphthalene degradation.[48] Members of the genera *Citrobacter* and *Serratia* have been associated with surfactant production where biodegradation of hydrocarbons is active.[49,50] Lastly, members of the assigned phylotypes *Streptococcus* and *Staphylococcus* have been associated with aerobic heavy alkane biodegradation.[51]

In contrast, the low-k zone showed an active microbial community reflective of anoxic conditions primarily composed of anaerobic fermenting bacteria and methanogenic archaea. Within the bacterial population, 63% of phylotypes were assigned as unclassified clostridia, which are generally known as strict anaerobes; in addition, some members of this class have the ability to degrade hydrocarbons synergistically with various methanogenic archaea.[52−54] Other anaerobic fermenters previously associated with hydrocarbon fermentation were identified, including *Pelotomaculum*,[55] *Firmicutes*,[56] *Smithella*,[56] and unclassified *Anaerolineaceae*.[57] Turning to the archaeal population in the anoxic low-k zone, 96% of the active Archaea identified were methanogens, of which 75% are associated with tolerance to oxygen exposure. The most abundant oxygen-tolerant archaeal phylotypes included members of the genera *Methanoregula* (52%)[58] and *Methanolinea* (19%). These methanogens are likely associated with methanogenic hydrocarbon degradation.[55,59,60]

The active microbial community in the oxic transmissive zone established a basis for aerobic hydrocarbon biodegradation. In the low-k zone, the active microbial community composition generally established a basis for anoxic conditions but also raised some questions regarding metabolic aspects in relation to the redox conditions and molecular formulas determined by FT-ICR MS (see below). The co-occurrence of strict anaerobes and oxygen-tolerant methanogens in the anoxic low-k zone at first glance may appear contradictory. A likely explanation for this observation is the assembly of microeconiche environments within a heterogeneous geological backdrop and fluctuating water level as visible in Figure 1.[61] Furthermore, we infer from this microbial community analysis the likelihood of syntrophic interactions among microbial populations to drive methanogenic hydrocarbon degradation in the anoxic low-k zone.[62] Lastly, given the age of the petroleum LNAPL body at this site, it is also possible that a portion of the phylotypes detected may not be directly involved with anaerobic hydrocarbon degradation but rather participate in synergistic, peripheral metabolic processes. In conclusion, our results highlight the significance of the interconnected governance of microbial ecology and biogeochemical environments underpinning late-stage hydrocarbon release sites.

Petroleum Biodegradation Metabolites Have a Higher Degree of Oxygenation under Anoxic Conditions. Two subsamples from the same depth as the two subsamples for microbial community analysis were selected for ultrahigh-resolution FT-ICR MS analyses of hydrocarbons and their biodegradation metabolites. Totals of 10 311 peaks and 8178 peaks were assigned elemental compositions with ∼0.2 ppm mass measurement accuracy in the anoxic low-k zone and oxic transmissive zone samples in negative-ion ESI, respectively. Figure 3 shows the heteroatom class distribution for acidic

https://doi.org/10.1021/acs.energyfuels.1c02642
Energy Fuels 2021, 35, 16713−16723

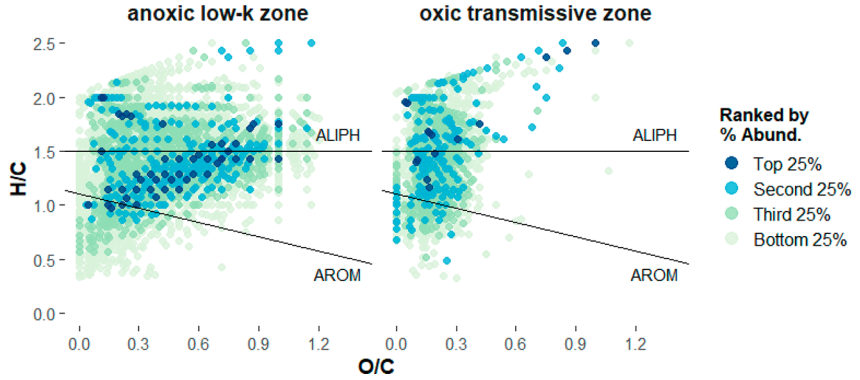

Figure 4. Van Krevelen diagrams for the anoxic low-k zone and oxic transmissive zone samples, highlighting the global shift in H/C versus O/C ratios for all assigned O_x and N_1O_x species identified by (−)ESI FT-ICR MS. Species with a modified aromaticity index >0.5 were designated aromatic (AROM), while formulas with H/C ratios ≥1.5 were designated aliphatic (ALIPH) according to Young et al. in 2018.[72]

species derived from negative-ion ESI FT-ICR MS. In both zones, the highest relative abundance was observed for the O_2 class, which includes species with a carboxylic acid functional group.[12] Crude oil can naturally contain hydrocarbon species with a low number of oxygen atoms. Both abiotic and biotic transformation processes ("weathering") are expected to lead to a transient increase in oxygenation on the path to full mineralization.[63−66]

Surprisingly, the ultrahigh-resolution mass spectra revealed a substantially higher degree of oxygenation in the biodegradation metabolites from the anoxic low-k zone compared to the oxic transmissive zone. In the oxic zone, relative abundances among oxygen-containing classes steadily decreased from the maximum at O_2, without detections above 10 oxygen atoms. In contrast, a second maximum was found in the anoxic low-k zone for the O_5 class, and species with up to 20 oxygen atoms were observed. Oil-extractable acidic compounds within the oxic transmissive zone correspond to compounds isolated in weathered oil,[12] whereas more oxygen-rich compounds in the anoxic zone correspond to heavily degraded oil-soluble compounds that are interfacially active.[67] We reiterate that discriminatory sample extraction with toluene was performed to minimize detections of natural organic matter, which may sometimes interfere with high-resolution hydrocarbon analysis.[20,26]

The microbial generation of highly oxidized hydrocarbon biodegradation metabolites with 20 oxygen atoms in the absence of molecular oxygen is mechanistically unprecedented. Anaerobic hydrocarbon degradation is most commonly associated with pathways such as fumarate addition, hydroxylation, carboxylation, or alternative anaerobic respiratory processes (e.g., denitrification and sulfate reduction) in addition to methanogenic hydrocarbon degradation.[68] Two potential scenarios can be provided to explain the observed speciation. First, groundwater solutes and contaminants are known to diffuse from highly transmissive zones into low-k zones.[11] It appears possible that highly diffusive oxygen was transported from the oxic transmissive zone into the (overall) anoxic low-k zone to a limited extent. Consequently, some aerobic transformation of petroleum hydrocarbons may be enabled, albeit at a substantially lower rate compared to the oxic transmissive zone where a constant high influx of river-derived dissolved oxygen leads to the rapid and complete mineralization of petroleum hydrocarbons without the accumulation of highly oxygenated intermediates. The high relative abundance of oxygen-tolerant Archaea in the anoxic low-k zone supports this conclusion. Second, some of the highly oxygenated compounds may not be direct hydrocarbon biodegradation products but rather cellular components such as biosurfactants that may aid in hydrocarbon degradation or lipid macromolecules.[69] Our results demonstrate the power of coupling microbial community composition analysis and FT-ICR MS on cryogenically collected core both to gain novel insights and to provide guidance for further investigation of hydrocarbon fate in the subsurface that can be used for site management.

Detections of pyrrolic nitrogen (N_1) and deprotonated hydrocarbon (HC) compounds were observed in both zones. These species correspond to five-member ring hydrocarbons (fluorene) and carbazoles that are prevalent in petroleum and can be deprotonated at the bridgehead carbon in negative-ion ESI with tetramethylammonium hydroxide solvent modification.[44] In crude oil, N_1 species have previously been reported as the major heteroatom class.[12,65,66,70] In both oxic and anoxic zone samples, the N_1O_6 class had the highest relative abundance among nitrogen-containing classes, implying that the hydrocarbons in both oxic transmissive and anoxic low-k zones had undergone oxidative transformation processes to a similar extent. We note that the higher relative abundances of N_1O_x classes in the oxic transmissive zone do not translate into higher absolute concentrations. Relative abundances of N_1O_x classes in the anoxic low-k zone sample were likely biased by the dominant O_x compounds. Likewise, while slightly higher oxygenated N_1O_x classes were detected in the anoxic low-k zone with up to N_1O_{20} versus N_1O_{17} in the oxic transmissive zone, ion suppression may have caused low-abundance compounds to fall below the peak detection limit.

Finally, mass spectra collected using positive-ion APPI supported the presence of nonoxygenated hydrocarbons as quantified by TPH analysis but showed only minor differences in less polar HC, O_x, and S_1 classes between the two hydrogeologic zones (Figure S2).

Both Aliphatic and Aromatic Hydrocarbons Are Biodegraded. The higher degree of oxygenation of the petroleum hydrocarbon metabolites from the anoxic low-k zone was further revealed through van Krevelen diagrams in Figure 4, which illustrate the degree of oxygenation (O/C ratio) vs degree of aromaticity (H/C ratio) for acidic species in the O_x and N_1O_x classes identified by (−)ESI FT-ICR MS in the oxic and anoxic toluene-soluble residues. Each dot on these graphs represents molecular formulas of the same O/C and H/C ratios assigned from the mass spectra.[71] The color-coding

https://doi.org/10.1021/acs.energyfuels.1c02642
Energy Fuels 2021, 35, 16713−16723

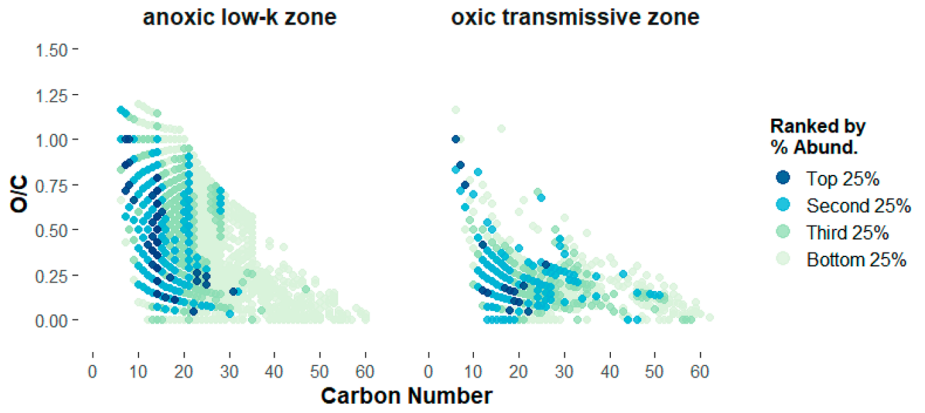

Figure 5. O/C ratio versus carbon number plots identifying elemental compositions of the assigned O_x and N_1O_x species identified by (−)ESI FT-ICR MS in samples from the anoxic low-k and oxic transmissive zones.

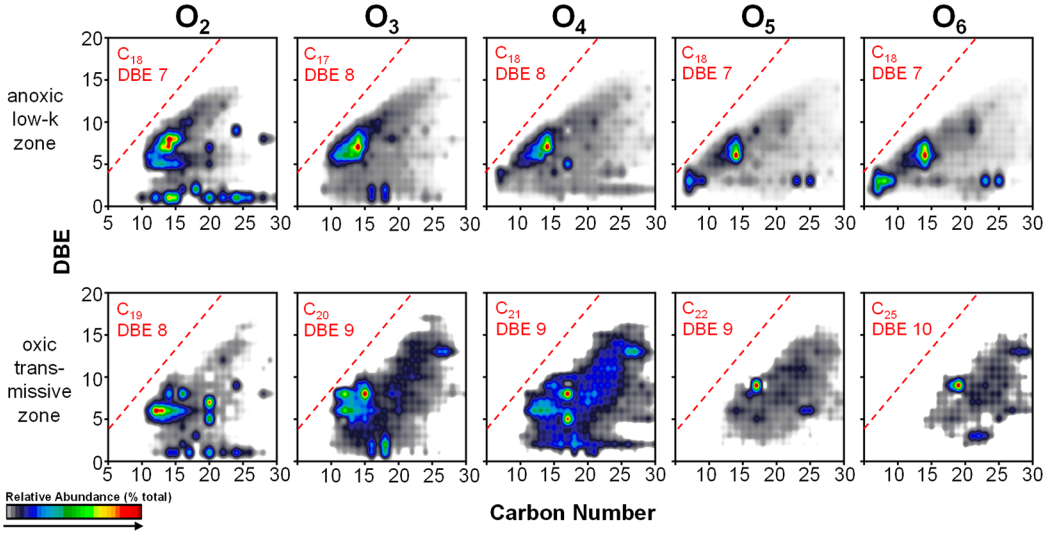

Figure 6. Isoabundance color-coded contoured plots of double bond equivalents (DBEs) versus carbon number for O_2−O_6 compounds derived from (−)ESI FT-ICR MS. A red dashed line marks the planar stability line for molecules to remain in a condensed phase. Compounds close to the planar limit line exhibit minimal alkylation and correspond to bare aromatic heterocycles.[78] Relative abundance-weighted average carbon number and DBE are shown in red for each image and show a slight increase in carbon number and DBE as a function of heteroatom content.

corresponds to the relative peak intensity of the compounds after normalization to the most abundant peak.

The two samples had similar H/C ranges, covering both aliphatic (high H/C ratio) and aromatic species (low H/C ratio). However, in the oxic zone, the acidic compounds had a narrow distribution of O/C ratios largely below 0.5, with the most abundant compounds between an O/C ratio of 0.1 and 0.2. The anoxic compounds spanned a wider range of O/C ratios, with highly abundant compounds at O/C ratios of 0.1−1.0. The observed minor changes in H/C ratios along with notable changes in O/C ratios indicate that initial oxidation reactions generate a diverse range of metabolites, in agreement with observations of petroleum hydrocarbon transformation in sediments impacted by the 2010 Deepwater Horizon oil spill.[12]

Both Low- and High-Molecular Weight Hydrocarbons Are Biodegraded. It has previously been proposed that C_{10}−C_{24} *n*-alkanes are more readily biodegradable, while species with less than 10 carbon atoms may be toxic to microorganisms, and species with more than 24 carbon atoms experience reduced transport across cell membranes.[73] The O/C ratio versus carbon number plots of all identified elemental compositions in the O_x and N_1O_x classes identified by (−)ESI FT-ICR MS shown in Figure 5 reveal that the observed increase in oxygen content in the anoxic low-k zone occurred across a broad carbon number range between at least C_6 and C_{35}. The relative abundance-weighted average carbon number in the oxic transmissive zone was 20.0, compared to an average of 16.9 in the anoxic low-k zone. The shift in carbon number with progressing oxidation at this late-state release site implies a (partial) breakdown of petroleum hydrocarbons across a range much broader than C_{10}−C_{24}.

Lower-Molecular Weight Aliphatic Species Are Completely Biodegraded under Aerobic Conditions. Finally, we characterized the compositional space of petroleum-derived metabolites by double bond equivalents (DBEs) versus the carbon number. DBEs are the number of rings plus double bonds in a molecule, calculated for compounds devoid of halogen atoms as shown in Figure 6 *via*:[74]

$$\mathrm{DBE} = C - \frac{H}{2} + \frac{N}{2} + 1 \quad (1)$$

In these plots, the *x*-axis reflects the molecular size and the *y*-axis reflects the degree of alkylation or aromaticity. In general, for any carbon number, the lower DBE numbers correspond to

https://doi.org/10.1021/acs.energyfuels.1c02642
Energy Fuels 2021, 35, 16713−16723

more aliphatic hydrocarbons while higher DBE numbers represent more unsaturated or aromatic species. The dashed red planar stability limit symbolizes the theoretical maximum DBE for planar polycyclic aromatic hydrocarbons, representing the theoretical limit between a planar and bowl-shaped structure.[18,75] These plots can highlight structural changes when comparing the same heteroatom class for two different samples.

Across both anoxic and oxic hydrogeologic zones, acidic compounds in the O_2−O_6 classes span between carbon numbers of 10 and 30. A bimodal distribution with DBE values between 1 and 3 and between 6 and 9 suggests multiple types of hydrocarbon sources/products. The O_2 class suggests molecules with a carboxylic acid functional group,[12] likely fatty acids at a DBE value of 1 as well as naphthenic and aromatic acids at DBE values greater than 1.[65,76] These species occur naturally in crude oil but may also be initial transformation products during the biodegradation of hydrocarbons.[65,77] Only minute differences in O_2 compositional space were visible between the two hydrogeologic zones in negative-ion ESI mode as well as in more nonpolar species detected in positive-ion APPI mode (Figure S3), suggesting that their speciation was strongly impacted by the residual oil phase.

However, differences between the samples from the low-k and transmissive zones begin to emerge with increasing degree of oxygenation. In the anoxic low-k zone, the relative abundance-weighted average DBE values and number of carbon atoms remained largely constant around 7−8 and 17−18, respectively. Analytes with the greatest abundance as indicated by a dark red color were consistently observed at a DBE values between 6 and 7 and a carbon number of 13. Supported by the broad distribution of carbon numbers over a wide range of O/C ratios in Figure 5, these results imply multiple partial oxygenation reactions of the hydrocarbons, for instance through hydroxylation, without carbon cleavage or diminishing the unsaturated nature of the species. In contrast, a shift toward a higher average DBE value of 10 and a higher average carbon number of 25 was observed in the O_3−O_6 classes from the oxic transmissive zone. Analytes with the greatest abundance were observed at higher DBE values between 8 and 9 and higher carbon numbers between 15 and 18 compared to those in the anoxic low-k zone. In conjunction with the active microbial community identified in the oxic transmissive zone, these data support the preferential and complete biodegradation of lower-molecular weight aliphatic species in the presence of oxygen as the electron acceptor.

CONCLUSIONS

Our molecular-level investigations of the transmissive and low-k zones in a heterogeneous aquifer offer a unique and astounding first glimpse at a late-stage petroleum hydrocarbon release site. At this particular study site, petroleum hydrocarbons in the anoxic low-k zone must be primarily biodegraded under methanogenic conditions. However, a small diffusive influx of molecular oxygen from river water recharge in the oxic transmissive zone likely leads to limited aerobic metabolism and the accumulation of highly oxygenated metabolites. In contrast, more abundant O_2 in the transmissive zone enables the rapid aerobic mineralization of petroleum hydrocarbons without the accumulation of highly oxygenated species. Biodegradation processes are active for a broad range of petroleum hydrocarbons, from aliphatic to aromatic compounds as well as from low- to high-molecular weight components.

At the same time, we acknowledge that this first (ultra)high-resolution attempt at characterizing a late-stage petroleum hydrocarbon release site bears limitations that raise additional questions to be addressed in future studies. First, the application of FT-ICR MS herein is a powerful qualitative analytical technique, and relative analyte abundances do not translate into absolute concentrations of the identified species. Rather, these data show compositional shifts and highlight similarities and differences between samples. The inherent difference in the ionization efficiency between different classes or mass-dependent ionization efficiency differences within a given class may obscure comparisons between relative concentrations of different classes.[79] Second, the ultimate fate of the identified petroleum hydrocarbon biodegradation metabolites at this site cannot be conclusively deduced from our findings. However, the biodegradation of more persistent naphthenic acids has been shown to occur under both aerobic and anaerobic conditions.[80,81] Additional analyses of samples over time and downgradient of the collected soil core would be desirable to confirm findings of previous studies that have reported the complete attenuation and mineralization of petroleum hydrocarbon metabolites once the residual LNAPL is fully depleted.[13,82,83]

Nevertheless, our work is a critical first step toward enabling better-informed decision making regarding best management practices for late-stage petroleum hydrocarbon-impacted sites.

ASSOCIATED CONTENT

Supporting Information

The Supporting Information is available free of charge at https://pubs.acs.org/doi/10.1021/acs.energyfuels.1c02642.

Table of acronyms and abbreviations list and figures of documentation of cryogenic core collection, heteroatom class distribution, and isoabundance color-coded contoured plots (PDF)

AUTHOR INFORMATION

Corresponding Author

Jens Blotevogel − *Department of Civil and Environmental Engineering, Colorado State University, Fort Collins, Colorado 80523, United States;* orcid.org/0000-0002-2740-836X; Phone: +1-970-491-8880; Email: jens.blotevogel@colostate.edu

Authors

Olivia K. Bojan − *Department of Civil and Environmental Engineering, Colorado State University, Fort Collins, Colorado 80523, United States;* Present Address: Geosyntec Consultants, Lakewood, CO 80228, United States

Maria Irianni-Renno − *Department of Civil and Environmental Engineering, Colorado State University, Fort Collins, Colorado 80523, United States*

Andrea J. Hanson − *Department of Civil and Environmental Engineering, Colorado State University, Fort Collins, Colorado 80523, United States;* orcid.org/0000-0003-2689-9870

Huan Chen − *National High Magnetic Field Laboratory, Florida State University, Tallahassee, Florida 32310, United States;* orcid.org/0000-0002-6032-6569

Robert B. Young − *Department of Soil & Crop Sciences, Colorado State University, Fort Collins, Colorado 80523, United States*

Susan K. De Long − *Department of Civil and Environmental Engineering, Colorado State University, Fort Collins, Colorado 80523, United States;* orcid.org/0000-0002-3160-2392

Thomas Borch − *Department of Civil and Environmental Engineering, Colorado State University, Fort Collins, Colorado 80523, United States; Department of Soil & Crop Sciences and Department of Chemistry, Colorado State University, Fort Collins, Colorado 80523, United States;* orcid.org/0000-0002-4251-1613

Thomas C. Sale − *Department of Civil and Environmental Engineering, Colorado State University, Fort Collins, Colorado 80523, United States*

Amy M. McKenna − *National High Magnetic Field Laboratory, Florida State University, Tallahassee, Florida 32310, United States; Department of Soil & Crop Sciences, Colorado State University, Fort Collins, Colorado 80523, United States;* orcid.org/0000-0001-7213-521X

Complete contact information is available at: https://pubs.acs.org/10.1021/acs.energyfuels.1c02642

Notes

The authors declare no competing financial interest.

■ ACKNOWLEDGMENTS

Funding for this project was provided by the University Consortium for Field-Focused Groundwater Research and the Ion Cyclotron Resonance User facility at the National High Magnetic Field Laboratory, which is supported by the National Science Foundation Division of Chemistry and Division of Materials Research through DMR 16-44779, and the State of Florida. The authors thank Cathelyne Powers at Colorado State University for graphical support with gINT plots.

■ REFERENCES

(1) Baedecker, M. J.; Cozzarelli, I. M.; Eganhouse, R. P.; Siegel, D. I.; Bennett, P. C. Crude oil in a shallow sand and gravel aquifer-III. Biogeochemical reactions and mass balance modeling in anoxic groundwater. *Appl. Geochem.* **1993**, *8*, 569−586.

(2) Bekins, B. A.; Cozzarelli, I. M.; Erickson, M. L.; Steenson, R. A.; Thorn, K. A. Crude oil metabolites in groundwater at two spill sites. *Groundwater* **2016**, *54*, 681−691.

(3) Essaid, H. I.; Bekins, B. A.; Herkelrath, W. N.; Delin, G. N. Crude oil at the Bemidji site: 25 years of monitoring, modeling, and understanding. *Groundwater* **2011**, *49*, 706−726.

(4) Garg, S.; Newell, C. J.; Kulkarni, P. R.; King, D. C.; Adamson, D. T.; Renno, M. I.; Sale, T. Overview of natural source zone depletion: Processes, controlling factors, and composition change. *Groundwater Monit. Rem.* **2017**, *37*, 62−81.

(5) Amos, R. T.; Mayer, K. U.; Bekins, B. A.; Delin, G. N.; Williams, R. L. Use of dissolved and vapor-phase gases to investigate methanogenic degradation of petroleum hydrocarbon contamination in the subsurface. *Water Resour. Res.* **2005**, *41*, W02001.

(6) Irianni-Renno, M.; Akhbari, D.; Olson, M. R.; Byrne, A. P.; Lefevre, E.; Zimbron, J.; Lyverse, M.; Sale, T. C.; De Long, S. K. Comparison of bacterial and archaeal communities in depth-resolved zones in an LNAPL body. *Appl. Microbiol. Biotechnol.* **2016**, *100*, 3347−3360.

(7) Karimi Askarani, K.; Sale, T. C. Thermal estimation of natural source zone depletion rates without background correction. *Water Res.* **2020**, *169*, 115245.

(8) Sale, T.; Hopkins, H.; Kirkman, A. Managing risk at LNAPL sites. Frequently asked questions. *Soil and Groundwater Research Bulletin No. 18*, 2nd ed.; American Petroleum Institute, 2018.

(9) Huntley, D.; Beckett, G. D. Persistence of LNAPL sources: relationship between risk reduction and LNAPL recovery. *J. Contam. Hydrol.* **2002**, *59*, 3−26.

(10) McCoy, K.; Zimbron, J.; Sale, T.; Lyverse, M. Measurement of Natural Losses of LNAPL Using CO_2 Traps. *Groundwater* **2015**, *53*, 658−667.

(11) Yang, M.; Annable, M. D.; Jawitz, J. W. Back Diffusion from Thin Low Permeability Zones. *Environ. Sci. Technol.* **2015**, *49* (1), 415−422.

(12) Chen, H.; Hou, A.; Corilo, Y. E.; Lin, Q.; Lu, J.; Mendelssohn, I. A.; Zhang, R.; Rodgers, R. P.; McKenna, A. M. 4 Years after the Deepwater Horizon Spill: Molecular Transformation of Macondo Well Oil in Louisiana Salt Marsh Sediments Revealed by FT-ICR Mass Spectrometry. *Environ. Sci. Technol.* **2016**, *50*, 9061−9069.

(13) Zemo, D. A.; O'Reilly, K. T.; Mohler, R. E.; Magaw, R. I.; Espino Devine, C.; Ahn, S.; Tiwary, A. K. Life cycle of petroleum biodegradation metabolite plumes, and implications for risk management at fuel release sites. *Integr. Environ. Assess. Manage.* **2017**, *13*, 714−727.

(14) Zemo, D. A.; O'Reilly, K. T.; Mohler, R. E.; Tiwary, A. K.; Magaw, R. I.; Synowiec, K. A. Nature and estimated human toxicity of polar metabolite mixtures in groundwater quantified as TPHd/DRO at biodegrading fuel release sites. *Groundwater Monit. Rem.* **2013**, *33*, 44−56.

(15) *TPH Risk Evaluation at Petroleum-Contaminated Sites (TPHRisk-1)*; Interstate Technology & Regulatory Council, TPH Risk Evaluation Team: Washington, D.C., 2018.

(16) Mohler, R. E.; Ahn, S.; O'Reilly, K.; Zemo, D. A.; Espino Devine, C.; Magaw, R.; Sihota, N. Towards comprehensive analysis of oxygen containing organic compounds in groundwater at a crude oil spill site using GCxGC-TOFMS and Orbitrap ESI-MS. *Chemosphere* **2020**, *244*, 125504.

(17) Steenson, R.; Hellmann-Blumberg, U.; Elias, D.; Brown, K.; Fry, N.; Naugle, A.; Meillier, L.; Prowell, C. Petroleum Metabolites: Literature Review and Assessment Framework. https://www.waterboards.ca.gov/rwqcb2/publications_forms/documents/SF_WB_Petroleum_Metabolites.pdf (accessed 2021-03-27), San Francisco Bay Regional Water Quality Control Board.

(18) McKenna, A. M.; Nelson, R. K.; Reddy, C. M.; Savory, J. J.; Kaiser, N. K.; Fitzsimmons, J. E.; Marshall, A. G.; Rodgers, R. P. Expansion of the analytical window for oil spill characterization by ultrahigh resolution mass spectrometry: beyond gas chromatography. *Environ. Sci. Technol.* **2013**, *47*, 7530−7539.

(19) Zemo, D. A.; Foote, G. R. The technical case for eliminating the use of the TPH analysis in assessing and regulating dissolved petroleum hydrocarbons in ground water. *Groundwater Monit. Rem.* **2003**, *23*, 95−104.

(20) Islam, A.; Ahmed, A.; Hur, M.; Thorn, K.; Kim, S. Molecular-level evidence provided by ultrahigh resolution mass spectrometry for oil-derived DOC in groundwater at Bemidji, Minnesota. *J. Hazard. Mater.* **2016**, *320*, 123−132.

(21) Dvorski, S.E.-M.; Gonsior, M.; Hertkorn, N.; Uhl, J.; Müller, H.; Griebler, C.; Schmitt-Kopplin, P. Geochemistry of Dissolved Organic Matter in a Spatially Highly Resolved Groundwater Petroleum Hydrocarbon Plume Cross-Section. *Environ. Sci. Technol.* **2016**, *50*, 5536−5546.

(22) Johnson, R. L.; Brow, C. N.; Johnson, R. O.; Simon, H. M. Cryogenic core collection and preservation of subsurface samples for biomolecular analysis. *Groundwater Monit. Rem.* **2013**, *33*, 38−43.

(23) Kiaalhosseini, S.; Johnson, R. L.; Rogers, R. C.; Renno, M. I.; Lyverse, M.; Sale, T. C. Cryogenic core collection (C_3) from unconsolidated subsurface media. *Groundwater Monit. Rem.* **2016**, *36*, 41−49.

(24) Irianni-Renno, M.; Sale, T. C.; De Long, S. K. Advanced methods for RNA recovery from petroleum impacted soils. *MethodsX* **2021**, *8*, 101503.

(25) Olson, M.; De Long, S.; Irianni-Renno, M.; Clayton, W.; Sale, T.; Johnson, R. Evaluating Long-Term Impacts of Soil-Mixing Source-Zone Treatment using Cryogenic Core Collection: ESTCP Project ER-201587. https://apps.dtic.mil/sti/pdfs/AD1042959.pdf (accessed 2021-03-06).
(26) Dongbao, F.; Woods, J. R.; Kung, J.; Kingston, D. M.; Kotlyar, L. S.; Sparks, B. D.; Mercier, P. H. J.; McCracken, T.; Ng, S. Residual Organic Matter Associated with Toluene-Extracted Oil Sands Solids and Its Potential Role in Bitumen Recovery via Adsorption onto Clay Minerals. *Energy Fuels* **2010**, *24* (4), 2249−2256.
(27) Purcell, J. M.; Hendrickson, C. L.; Rodgers, R. P.; Marshall, A. G. Atmospheric Pressure Photoionization Fourier Transform Ion Cyclotron Resonance Mass Spectrometry for Complex Mixture Analysis. *Anal. Chem.* **2006**, *78* (16), 5906−5912.
(28) Robb, D. B.; Covey, T. R.; Bruins, A. P. Atmospheric pressure photoionisation: An ionization method for liquid chromatography mass spectrometry. *Anal. Chem.* **2000**, *72* (15), 3653−3659.
(29) Robb, D. B.; Blades, M. W. Factors affecting primary ionization in dopant-assisted atmospheric pressure photoionization (DA-APPI) for LC/MS. *J. Am. Soc. Mass Spectrom.* **2006**, *17* (2), 130−138.
(30) Smith, D. F.; Robb, D. B.; Blades, M. W. Comparison of dopants for charge exchange ionization of nonpolar polycyclic aromatic hydrocarbons with reversed-phase LC-APPI-MS. *J. Am. Soc. Mass Spectrom.* **2009**, *20* (1), 73−79.
(31) Purcell, J. M.; Rodgers, R. P.; Hendrickson, C. L.; Marshall, A. G. Speciation of nitrogen containing aromatics by atmospheric pressure photoionization or electrospray ionization Fourier transform ion cyclotron resonance mass spectrometry. *J. Am. Soc. Mass Spectrom.* **2007**, *18* (7), 1265−1273.
(32) Purcell, J. M.; Rodgers, R. P.; Hendrickson, C. L.; Marshall, A. G. Atmospheric pressure photoionization proton transfer for complex organic mixtures investigated by Fourier transform ion cyclotron resonance mass spectrometry. *J. Am. Soc. Mass Spectrom.* **2007**, *18*, 1682−1689.
(33) Lobodin, V. V.; Juyal, P.; McKenna, A. M.; Rodgers, R. P.; Marshall, A. G. Tetramethylammonium hydroxide as a reagent for complex mixture analysis by negative ion electrospray ionization mass spectrometry. *Anal. Chem.* **2013**, *85*, 7803−7808.
(34) Kaiser, N. K.; Quinn, J. P.; Blakney, G. T.; Hendrickson, C. L.; Marshall, A. G. A Novel 9.4 T FTICR mass spectrometer with improved sensitivity, mass resolution, and mass range. *J. Am. Soc. Mass Spectrom.* **2011**, *22* (8), 1343−1351.
(35) Blakney, G. T.; Hendrickson, C. L.; Marshall, A. G. Predator data station: A fast data acquisition system for advanced FT-ICR MS experiments. *Int. J. Mass Spectrom.* **2011**, *306* (2−3), 246−252.
(36) Senko, M. W.; Hendrickson, C. L.; Emmett, M. R.; Shi, S. D.-H.; Marshall, A. G. External accumulation of ions for enhanced electrospray ionization Fourier transform ion cyclotron resonance mass spectrometry. *J. Am. Soc. Mass Spectrom.* **1997**, *8*, 970−976.
(37) Wilcox, B. E.; Hendrickson, C. L.; Marshall, A. G. Improved ion extraction from a linear octopole ion trap: SIMION analysis and experimental demonstration. *J. Am. Soc. Mass Spectrom.* **2002**, *13*, 1304−1312.
(38) Tolmachev, A. V.; Robinson, E. W.; Wu, S.; Kang, H.; Lourette, N. M.; Pasa-Tolic, L.; Smith, R. D. Trapped-ion cell with improved DC potential harmonicity for FT-ICR MS. *J. Am. Soc. Mass Spectrom.* **2008**, *19* (4), 586−597.
(39) Kaiser, N. K.; Savory, J. J.; McKenna, A. M.; Quinn, J. P.; Hendrickson, C. L.; Marshall, A. G. Electrically compensated Fourier transform ion cyclotron resonance cell for complex mixture mass analysis. *Anal. Chem.* **2011**, *83* (17), 6907−6910.
(40) Xian, F.; Hendrickson, C. L.; Blakney, G. T.; Beu, S. C.; Marshall, A. G. Automated broadband phase correction of Fourier transform ion cyclotron resonance mass spectra. *Anal. Chem.* **2010**, *82* (21), 8807−8812.
(41) Xian, F.; Corilo, Y. E.; Hendrickson, C. L.; Marshall, A. G. Baseline correction of absorption-mode Fourier transform ion cyclotron resonance mass spectra. *Int. J. Mass Spectrom.* **2012**, *325* (327), 67−72.
(42) Kendrick, E. A mass scale based on CH_2 = 14.0000 for high resolution mass spectrometry of organic compounds. *Anal. Chem.* **1963**, *35*, 2146−2154.
(43) Hughey, C. A.; Hendrickson, C. L.; Rodgers, R. P.; Marshall, A. G.; Qian, K. Kendrick Mass Defect Spectrum: A Compact Visual Analysis for Ultrahigh-Resolution Broadband Mass Spectra. *Anal. Chem.* **2001**, *73*, 4676−4681.
(44) Savory, J. J.; Kaiser, N. K.; McKenna, A. M.; Xian, F.; Blakney, G. T.; Rodgers, R. P.; Hendrickson, C. L.; Marshall, A. G. Parts-per-billion Fourier transform ion cyclotron resonance mass measurement accuracy with a "walking" calibration equation. *Anal. Chem.* **2011**, *83* (5), 1732−1736.
(45) Corilo, Y. E. PetroOrg Software; Florida State University, Omics LLC: Tallahassee, Fl, 2014.
(46) Caporaso, J. G.; Lauber, C. L.; Walters, W. A.; Berg-Lyons, D.; Huntley, J.; Fierer, N.; Owens, S. M.; Betley, J.; Fraser, L.; Bauer, M.; et al. Ultra-high-throughput microbial community analysis on the Illumina HiSeq and MiSeq platforms. *ISME J.* **2012**, *6*, 1621−1624.
(47) Slapeta, J.; Linares, M. C. Combined amplicon pyrosequencing assays reveal presence of the apicomplexan "type-N"(cf. Gemmocystis cylindrus) and Chromera velia on the Great Barrier Reef, Australia. *PLoS One* **2013**, *8*, e76095.
(48) Godheja, J.; Shekhar, S. K.; Modi, D. R. Biodegradation of one ring hydrocarbons (benzene and toluene) and two ring hydrocarbons (acenapthene and napthalene) by bacterial isolates of hydrocarbon contaminated sites located in Chhattisgarh: A preliminary study. *J. Pet. Environ. Biotechnol.* **2015**, *6*, 202.
(49) Joy, S.; Rahman, P. K.; Sharma, S. Biosurfactant production and concomitant hydrocarbon degradation potentials of bacteria isolated from extreme and hydrocarbon contaminated environments. *Chem. Eng. J.* **2017**, *317*, 232−241.
(50) Holmberg, K. Natural surfactants. *Curr. Opin. Colloid Interface Sci.* **2001**, *6*, 148−159.
(51) Chaerun, S. K.; Tazaki, K.; Asada, R.; Kogure, K. Bioremediation of coastal areas 5 years after the Nakhodka oil spill in the Sea of Japan: Isolation and characterization of hydrocarbon-degrading bacteria. *Environ. Int.* **2004**, *30*, 911−922.
(52) Morris, B. E.; Henneberger, R.; Huber, H.; Moissl-Eichinger, C. Microbial syntrophy: Interaction for the common good. *FEMS Microbiology Reviews* **2013**, *37*, 384−406.
(53) Zeman, N. R.; Irianni Renno, M.; Olson, M. R.; Wilson, L. P.; Sale, T. C.; De Long, S. K. Temperature impacts on anaerobic biotransformation of LNAPL and concurrent shifts in microbial community structure. *Biodegradation* **2014**, *25*, 569−585.
(54) Fowler, S. J.; Toth, C. R.; Gieg, L. M. Community structure in methanogenic enrichments provides insight into syntrophic interactions in hydrocarbon-impacted environments. *Front. Microbiol.* **2016**, *7*, 562.
(55) Scherr, K. E.; Lundaa, T.; Klose, V.; Bochmann, G.; Loibner, A. P. Changes in bacterial communities from anaerobic digesters during petroleum hydrocarbon degradation. *J. Biotechnol.* **2012**, *157*, 564−572.
(56) An, D.; Brown, D.; Chatterjee, I.; Dong, X.; Ramos-Padron, E.; Wilson, S.; Bordenave, S.; Caffrey, S. M.; Gieg, L. M.; Sensen, C. W.; Voordouw, G. Microbial community and potential functional gene diversity involved in anaerobic hydrocarbon degradation and methanogenesis in an oil sands tailings pond. *Genome* **2013**, *56* (10), 612−618.
(57) Liang, B.; Wang, L. Y.; Mbadinga, S. M.; Liu, J. F.; Yang, S. Z.; Gu, J. D.; Mu, B. Z. Anaerolineaceae and Methanosaeta turned to be the dominant microorganisms in alkanes-dependent methanogenic culture after long-term of incubation. *AMB Express* **2015**, *5* (1), 1−13.
(58) Hunger, S.; Schmidt, O.; Gößner, A. S.; Drake, H. L. Formate-derived H_2, a driver of hydrogenotrophic processes in the root-zone of a methane-emitting fen. *Environ. Microbiol.* **2016**, *18*, 3106−3119.
(59) Toth, C. R. A.; Gieg, L. M. Time Course-Dependent Methanogenic Crude Oil Biodegradation: Dynamics of Fumarate Addition Metabolites, Biodegradative Genes, and Microbial Community Composition. *Front. Microbiol.* **2018**, *8*, 2610.

(60) Vigneron, A.; Cruaud, P.; Ducellier, F.; Head, I. M.; Tsesmetzis, N. Syntrophic Hydrocarbon Degradation in a Decommissioned Off-Shore Subsea Oil Storage Structure. *Microorganisms* **2021**, *9*, 356.
(61) Kleinsteuber, S.; Schleinitz, K. M.; Vogt, C. Key players and team play: anaerobic microbial communities in hydrocarbon-contaminated aquifers. *Appl. Microbiol. Biotechnol.* **2012**, *94*, 851−873.
(62) Gieg, L. M.; Fowler, S. J.; Berdugo-Clavijo, C. Syntrophic biodegradation of hydrocarbon contaminants. *Curr. Opin. Biotechnol.* **2014**, *27*, 21−29.
(63) Aeppli, C.; Carmichael, C. A.; Nelson, R. K.; Lemkau, K. L.; Graham, W. M.; Redmond, M. C.; Valentine, D. L.; Reddy, C. M. Oil Weathering after the Deepwater Horizon Disaster Led to the Formation of Oxygenated Residues. *Environ. Sci. Technol.* **2012**, *46* (16), 8799−8807.
(64) McKenna, A. M.; Chen, H.; Weisbrod, C. R.; Blakney, G. T. Molecular Comparison of Solid-Phase Extraction and Liquid/Liquid Extraction of Water-Soluble Petroleum Compounds Produced through Photodegradation and Biodegradation by FT-ICR Mass Spectrometry. *Anal. Chem.* **2021**, *93* (10), 4611−4618.
(65) Pan, Y.; Liao, Y.; Shi, Q. Variations of Acidic Compounds in Crude Oil during Simulated Aerobic Biodegradation: Monitored by Semiquantitative Negative-Ion ESI FT-ICR MS. *Energy Fuels* **2017**, *31* (2), 1126−1135.
(66) Ruddy, B. M.; Huettel, M.; Kostka, J. E.; Lobodin, V. V.; Bythell, B. J.; McKenna, A. M.; Aeppli, C.; Reddy, C. M.; Nelson, R. K.; Marshall, A. G.; Rodgers, R. P. Targeted Petroleomics: Analytical Investigation of Macondo Well Oil Oxidation Products from Pensacola Beach. *Energy Fuels* **2014**, *28* (6), 4043−4050.
(67) Zito, P.; Podgorski, D. C.; Bartges, T.; Guillemette, F.; Roebuck, J. A., Jr.; Spencer, R. G. M.; Rodgers, R. P.; Tarr, M. A. Sunlight-Induced Molecular Progression of Oil into Oxidized Oil Soluble Species, Interfacial Material, and Dissolved Organic Matter. *Energy Fuels* **2020**, *34* (4), 4721−4726.
(68) Widdel, F.; Rabus, R. Anaerobic biodegradation of saturated and aromatic hydrocarbons. *Curr. Opin. Biotechnol.* **2001**, *12*, 259−76.
(69) Ron, E. Z.; Rosenberg, E. Biosurfactants and oil bioremediation. *Curr. Opin. Biotechnol.* **2002**, *13*, 249−252.
(70) Shi, Q.; Hou, D.; Chung, K. H.; Xu, C.; Zhao, S.; Zhang, Y. Characterization of Heteroatom Compounds in a Crude Oil and Its Saturates, Aromatics, Resins, and Asphaltenes (SARA) and Non-basic Nitrogen Fractions Analyzed by Negative-Ion Electrospray Ionization Fourier Transform Ion Cyclotron Resonance Mass Spectrometry. *Energy Fuels* **2010**, *24*, 2545−2553.
(71) Kim, S.; Kramer, R. W.; Hatcher, P. G. Graphical method for analysis of ultrahigh-resolution broadband mass spectra of natural organic matter, the van Krevelen diagram. *Anal. Chem.* **2003**, *75* (20), 5336−5344.
(72) Young, R.; Avneri-Katz, S.; McKenna, A.; Chen, H.; Bahureksa, W.; Polubesova, T.; Chefetz, B.; Borch, T. Composition-Dependent Sorptive Fractionation of Anthropogenic Dissolved Organic Matter by Fe(III)-Montmorillonite. *Soil Syst.* **2018**, *2* (1), 14.
(73) Peters, K. E.; Walters, C. C.; Moldowan, J. M. *The Biomarker Guide, Biomarkers and Isotopes in Petroleum Exploration and Earth History*; Cambridge University Press: New York, 2005; pp 667−668.
(74) Vetter, W.; McLafferty, F. W.; Turecek, F. *Interpretation of Mass Spectra*, 4th ed.; University Science Books: Sausalito, CA, 1993; p 1379.
(75) Lobodin, V. V.; Marshall, A. G.; Hsu, C. S. Compositional Space Boundaries for Organic Compounds. *Anal. Chem.* **2012**, *84* (7), 3410−3416.
(76) Liao, Y. H.; Shi, Q.; Hsu, C. S.; Pan, Y. H.; Zhang, Y. H. Distribution of acids and nitrogen-containing compounds in biodegraded oils of the Liaohe Basin by negative ion ESI FT-ICR MS. *Org. Geochem.* **2012**, *47*, 51−65.
(77) Kim, S.; Stanford, L. A.; Rodgers, R. P.; Marshall, A. G.; Walters, C. C.; Qian, K.; Wenger, L. M.; Mankiewicz, P. Microbial alteration of the acidic and neutral polar NSO compounds revealed by Fourier transform ion cyclotron resonance mass spectrometry. *Org. Geochem.* **2005**, *36* (8), 1117−1134.
(78) Hsu, C. S.; Lobodin, V. V.; Rodgers, R. P.; McKenna, A. M.; Marshall, A. G. Compositional Boundaries for Fossil Hydrocarbons. *Energy Fuels* **2011**, *25* (5), 2174−2178.
(79) Hughey, C. A.; Rodgers, R. P.; Marshall, A. G.; Walters, C. C.; Qian, K.; Mankiewicz, P. *Org. Geochem.* **2004**, *35* (7), 863−880.
(80) Clothier, L. N.; Gieg, L. M. Anaerobic biodegradation of surrogate naphthenic acids. *Water Res.* **2016**, *90*, 156−166.
(81) Herman, D. C.; Fedorak, P. M.; MacKinnon, M. D.; Costerton, J. W. Biodegradation of naphthenic acids by microbial populations indigenous to oil sands tailings. *Can. J. Microbiol.* **1994**, *40*, 467−477.
(82) Barcelona, M. J.; Lu, J.; Tomczak, D. M. Organic acid derivatization techniques applied to petroleum hydrocarbon transformations in subsurface environments. *Groundwater Monit. Rem.* **1995**, *15*, 114−124.
(83) Langbehn, A.; Steinhart, H. Biodegradation studies of hydrocarbons in soils by analyzing metabolites formed. *Chemosphere* **1995**, *30*, 855−868.

https://doi.org/10.1021/acs.energyfuels.1c02642
Energy Fuels 2021, 35, 16713−16723